

FeynmanDD: Quantum Circuit Analysis with Classical Decision Diagrams

Ziyuan Wang^{*1}, Bin Cheng^{*2}, Longxiang Yuan¹, and Zhengfeng Ji^{**1,3}

¹ Department of Computer Science and Technology, Tsinghua University

² Centre for Quantum Technologies, National University of Singapore

³ Zhongguancun Laboratory

Abstract. Applications of decision diagrams in quantum circuit analysis have been an active research area. Our work introduces FeynmanDD, a new method utilizing standard and multi-terminal decision diagrams for quantum circuit simulation and equivalence checking. Unlike previous approaches that exploit patterns in quantum states and operators, our method explores useful structures in the path integral formulation, essentially transforming the analysis into a counting problem. The method then employs efficient counting algorithms using decision diagrams as its underlying computational engine. Through comprehensive theoretical analysis and numerical experiments, we demonstrate FeynmanDD’s capabilities and limitations in quantum circuit analysis, highlighting the value of this new BDD-based approach.

Keywords: Decision Diagrams · Quantum Computing · Classical Simulation of Quantum Circuits · Quantum Circuit Equivalence

1 Introduction

Binary Decision Diagrams (BDDs) are widely regarded as one of the most influential data structures for representing, analyzing, and simulating classical circuits [11, 38]. Since their introduction in the 1980s [10], BDDs have found applications in various domains, including circuit synthesis, formal verification, and model checking. In one of his video lectures given in the 2000s on trees and BDDs, Donald Knuth described them as “one of the few truly fundamental data structures that came out in the last twenty-five years”. In his seminal book series, *The Art of Computer Programming*, he dedicated an entire section to BDDs [31].

Given their success in classical circuit design and analysis, it is natural to explore how BDDs can be extended to the representation and simulation of quantum circuits. The core idea of decision diagrams is to exploit repeated patterns in truth tables, enabling compact data representations. Quantum states and operations, like truth tables, scale exponentially yet may also exhibit repetitive patterns. For example, directly representing an n -qubit state requires storing

^{*} First authors.

^{**} Correspondence author. Email: jizhengfeng@tsinghua.edu.cn.

2^n complex numbers, known as amplitudes. Several existing works in quantum computing adopt this approach to identify patterns in quantum states and operations [3, 12, 26, 30, 35, 41, 51, 52, 56, 61–63]. Some studies, like those in [29, 32], combine tensor network methods with decision diagrams to enhance computational efficiency. Others, such as [47], incorporate additional compression techniques based on context-free languages. These methods, inspired by BDDs, extend beyond traditional BDDs and are better described as *BDD-motivated* techniques.

In BDD-motivated approaches, entirely new implementations of the data structure are often required. Additionally, to capture more intricate patterns, non-trivial labels may need to be assigned to the diagram’s links [29, 41, 62, 63]. In contrast, a less-explored approach uses classical BDD data structures and decision diagram packages, such as CUDD [49], to directly represent and manipulate quantum states. For example, Ref. [50] proposed a bit-slicing method to represent quantum amplitudes of states generated by the Clifford and T gate set using BDDs. We refer to this as a *BDD-based* method, as it utilizes classical BDDs as the underlying engine. Given the limited research on BDD-based methods for quantum circuits, a natural question arises: *Are there other BDD-based methods that can significantly enhance the analysis and simulation of quantum circuits?*

Key Contributions. We answer this question in the affirmative by proposing a new BDD-based method.

The first key contribution is the novel integration of the counting capabilities of decision diagrams in quantum circuit analysis. The profound connection between counting and quantum computing [1, 21, 57] is well-established, with counting complexity classes providing natural upper bounds for BQP [57] and underpinning quantum supremacy schemes [1]. While the counting perspective has been explored in quantum circuit analysis [37], this work uniquely combines quantum circuits’ counting nature with BDDs’ efficient counting algorithms. When decision diagrams have bounded size, counting solutions becomes efficient—a key advantage of BDDs highlighted in Knuth’s book [31]. This counting algorithm then serves as the computational engine in our method. Unlike traditional Schrödinger-style simulators that use specialized BDD variants for state vector evolution [29, 41, 50, 62, 63], our method explores structures in the Feynman-type exponential sums. To emphasize its foundations in Feynman path integral, we name our method *FeynmanDD* (Feynman Decision Diagrams).

The second contribution encompasses efficiency-enhancing techniques. We present a binary synthesis method for constructing FeynmanDD’s underlying decision diagram, carefully transforming low-degree multilinear polynomials to BDDs through strategic term ordering. This approach reduces both intermediate representation sizes and computational complexity. We also emphasize the importance of variable ordering for BDDs, providing various ordering heuristics for different circuit families. The combined consideration of term orders and variable orders proves crucial for the overall efficiency of our method. Furthermore, we introduce a sum-of-powers framework that is both flexible—supporting multiple

gate sets within a unified approach—and efficient, as it delays conversion to BDDs, further optimizing performance.

Finally, extensive numerical experiments demonstrate the superior performance of FeynmanDD compared to existing decision diagram tools like DDSIM and SliQSim in amplitude computation while showing advantageous performance in sampling tasks for many families of circuit types even though our sampling efficiency does not match that for amplitude estimation. FeynmanDD also proves effective for circuit equivalence checking for certain families of circuits, with performance comparable to its simulation capabilities. These results confirm that FeynmanDD represents a promising new direction in quantum circuit analysis that is worthy of further investigation. In a follow-up work, we will provide a characterization of the complexity of the FeynmanDD method, showing provable efficiency advantages over tensor network methods for certain families of circuits.

Outline. We develop a sum-of-powers (SOP) framework to handle diverse quantum gate sets in Section 3, consistently mapping circuits of different discrete quantum gate sets into SOP forms. As special cases of tensor networks, SOPs can be manipulated and simplified using tensor techniques, which we explain in Section 4. Converting a quantum circuit to its SOP representation is straightforward. The challenge lies in representing the SOP function f as a BDD (or multi-terminal BDD [9]), which is carefully discussed in Section 5. After constructing the BDD for f_C , we demonstrate in Section 6 how FeynmanDD enables quantum circuit analysis and simulation, including amplitude computation, measurement outcome sampling, and circuit equivalence checking. To initiate a rigorous understanding of FeynmanDD’s capabilities, we construct circuits using the linear network construction in [31] (Figure 23), which FeynmanDD can simulate efficiently, while tensor network and Clifford methods face provably high complexity. Extensive numerical experiments on quantum circuit simulation and equivalence checking are conducted and discussed in Section 7 and Section 8 respectively.

2 Preliminaries

2.1 Basics of Quantum Circuits

This work focuses on pure quantum states and does not consider noise and mixed states. An n -qubit pure quantum state is a normalized vector in the Hilbert space \mathbb{C}^{2^n} , denoted as $|\psi\rangle = \sum_{x \in \{0,1\}^n} c_x |x\rangle$, where $|x\rangle$ represents the computational basis. Quantum circuits describe the evolution of quantum states through sequences of unitary operators, typically acting on one, two, or three qubits. Important quantum gates include the Hadamard gate $H = \frac{1}{\sqrt{2}} \begin{pmatrix} 1 & 1 \\ 1 & -1 \end{pmatrix}$,

the Pauli-Z gate $Z = \begin{pmatrix} 1 & 0 \\ 0 & -1 \end{pmatrix}$, the controlled-Z gate (CZ), and the controlled-controlled-Z gate (CCZ). These gates form a weak universal set capable of approximating any (real) unitary operator to arbitrary precision and sufficient to simulate all quantum computation. Other gates are also considered in this work

and are discussed in Section 3. Our analysis considers quantum circuits acting on initial state $|0^n\rangle$ without loss of generality. With U denoting the circuit’s unitary operator, the final measurement in the computational basis yields a classical string $x \in \{0, 1\}^n$ with probability $|\langle x|U|0^n\rangle|^2$.

2.2 Quantum Circuit Analysis

There are several types of quantum circuit analysis tasks widely considered in the literature, including circuit simulation, equivalence checking, circuit synthesis and optimization. Our method is currently applicable to the simulation and equivalence-checking tasks.

As our equivalence checking method is reduced to a variant of circuit simulation in the end, we will focus on the discussion of quantum circuit simulation here. There are two notions for classical simulation of quantum circuits: the strong simulation and the weak simulation. The strong simulation requires computing the output amplitude $\langle x|U|0^n\rangle$ (or the output probability) given x and U . The weak simulation requires sampling from the output distribution of the quantum circuit, i.e., returning a string x with probability $|\langle x|U|0^n\rangle|^2$.

A straightforward way to simulate quantum circuits is to use the Schrödinger method, where the quantum state is stored as a 2^n -dimensional vector [33]. The quantum gates are represented by $2^n \times 2^n$ matrices, and the quantum state is updated by matrix-vector multiplication. Since the quantum state is stored, both the strong and weak simulations can be performed. The Schrödinger method requires exponential space and time complexity, which quickly becomes infeasible for large quantum circuits.

Another classical simulation technique is based on the Feynman path integral [23]. Suppose U consists of m gates, $U = U_m \cdots U_2 U_1$. Then, the idea of Feynman path integral is to insert identity operators in between, transforming the output amplitude into an exponential sum of products:

$$\langle x|U|0^n\rangle = \sum_{y_1, \dots, y_{m-1} \in \{0, 1\}^n} \langle x|U_m|y_{m-1}\rangle \cdots \langle y_2|U_2|y_1\rangle \langle y_1|U_1|0^n\rangle. \quad (1)$$

Note that each matrix element in the summation can be directly obtained from the specification of the corresponding gate. For some universal gate sets, these matrix elements can be represented by a particularly simple form, giving a sum-of-powers representation as detailed in Section 3. This simulation method has polynomial space complexity but the time complexity is exponential in the *number of gates*, which is even worse than the Schrödinger method.

Instead of directly computing the summation in Eq. (1), one can also compute it by tensor network contraction, one of the state-of-the-art classical simulation techniques [36, 42]. A rank- k tensor with bond dimension two can be represented by a 2^k -dimensional array, f_{i_1, \dots, i_k} , where $i_1, \dots, i_k \in \{0, 1\}$. In this way, a single- or two-qubit gate can be represented by a rank-2 or rank-4 tensor, respectively. A tensor network is a collection of tensors, where each index may appear in one or two tensors. The contraction of a tensor network is to sum over all indices

that shared by two tensors. For tensor network representation of the amplitude $\langle x|U|0^n\rangle$, no open wires remain and all indices appearing in the tensor network are summed over, giving a scalar of interest. In this work, we explore BDD-based techniques for Feynman-type simulation. We briefly mention that other families of techniques beyond decision diagrams have also been studied in the literature including, for example, phase polynomials [5, 40], tensor-based techniques [36, 42], ZX calculus [15, 16, 59], and tree automata [4, 14].

2.3 Binary Decision Diagrams

A binary decision diagram is a rooted, directed acyclic graph that succinctly represents Boolean functions. It contains two node types: decision nodes and terminal nodes. Each decision node carries a variable label, such as x_i , with two outgoing links to child nodes. The dashed link represents the branch for $x_i = 0$, while the solid link represents $x_i = 1$. The terminal nodes, valued as 0 and 1, represent the function’s output values. Any path from the root to a terminal node corresponds to a specific variable assignment, with the terminal node indicating the Boolean function’s value for that assignment. An example of a BDD is shown in Fig. 2.

Two additional properties of BDDs are important: being ordered and reduced. An *ordered* BDD ensures that variables appear in a consistent order along all paths from the root to terminal nodes. A *reduced* BDD contains no isomorphic subgraphs and no node has identical children. In the literature, BDDs typically refer to reduced ordered BDDs (ROBDDs), which provide a canonical representation of Boolean functions. This work employs multi-terminal BDDs (MTBDDs), also known as Algebraic Decision Diagrams (ADDs) [9], a generalized version where terminal nodes can take multiple values rather than just binary values.

For a Boolean function f , we denote $B(f)$ as the number of nodes in its BDD representation. Once a compact BDD representation is found for f , many problems related to the function become tractable, with time complexity polynomial in $B(f)$, even if they were computationally hard originally. Notably, counting solutions for $f(x) = 1$ using BDD requires time linear in $B(f)$ [31, 58]. Therefore, when $B(f)$ remains polynomially bounded, such counting operations can be performed efficiently. It is well-known that the variable ordering significantly impacts the BDD size, and that finding the optimal ordering is known to be NP-hard [58]. Most BDD packages provide dynamic variable ordering heuristics [45] which is useful for our purpose.

3 Sum-of-Powers Representation for Quantum Circuits

We begin our exposition by introducing the sum-of-powers (SOP) representation, derived from the Feynman path integral formalism, which emerges as a flexible framework for quantum circuit analysis; see, e.g., [6, 7, 13, 19, 53–55]. The SOP approach utilizes the fact that there exist universal gate sets consisting of unitary gates with particularly simple forms—so simple that all non-zero entries of the

unitary matrix have values proportional to the *power* $\omega^{f(x_1, x_2, \dots, x_k)}$, where ω is some root of unity and x_1, x_2, \dots, x_k are variables labeling the input and output wires discussed later. This method has been explored in several quantum computing works, initially by [18] and subsequently by [39]. Here, we review and slightly extend this approach within the SOP framework.

3.1 Gate Set \mathcal{Z}

First, consider quantum circuits over the gate set $\mathcal{Z} = \{H, Z, CZ, CCZ\}$. As in [39], we will label the wires of the circuit using the following method. Initially, we introduce a new variable for each qubit to label its corresponding wire. Subsequently, each Hadamard gate creates an additional variable to label its output wire, which is the only way a new variable can be generated. For a circuit with n qubits and h Hadamard gates, the total number of variables will be $n + h$. A labeling example is given in the left part in Fig. 1, where the circuit consists of four H gates, one Z gate, one CZ gate, and two CCZ gates. In this circuit, seven variables x_1, x_2, \dots, x_7 label the circuit wires where x_1, x_2, x_3 represent the initial three qubits and x_4, \dots, x_7 are introduced by the four H gates.

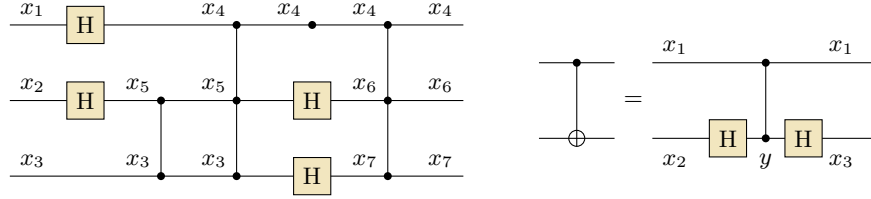


Fig. 1. Left: Variable labeling for a quantum circuit of gates from gate set \mathcal{Z} . Right: A decomposition that derives a power-of-sum representation for CNOT.

The H gate has matrix entries $(-1)^{xy}/\sqrt{2}$ where x and y are the variables for the input and output wires respectively. The CCZ gate has diagonal entries of $(-1)^{x_1x_2x_3}$ with 0 entries elsewhere, using the same set of variables for the input and output to indicate its diagonal nature. In the example of Fig. 1, the top qubit's H gate is represented as the power $(-1)^{x_1x_4}/\sqrt{2}$ and the final CCZ gate is represented by $(-1)^{x_4x_6x_7}$. The gates CZ and Z can be discussed similarly with fewer variables. Notice that, in this example, all gates in \mathcal{Z} are represented by powers of -1 up to a normalization factor (for H).

The power forms of the gates in the set \mathcal{Z} can be identified as a special tensor. For H, it is a tensor of two legs labeled by variables x, y , and for given values $x, y \in \{0, 1\}$, the tensor takes value $(-1)^{xy}/\sqrt{2}$. The gate CCZ is a tensor of six legs where three of them x_1, x_2, x_3 are input and other three y_1, y_2, y_3 are output. This tensor takes value zero if input variables (x_1, x_2, x_3) and output variables (y_1, y_2, y_3) differ, and $(-1)^{x_1x_2x_3}$ when they are identical. This explains the reason we use the same set of variables for CCZ in the labeling which enforces

the input-output variable equality. Consequently, each gate in \mathcal{Z} is mapped to a tensor of the power form, and each variable represents either the external (input and output) variables or internal variables that are summed over by the tensor network contraction operation. For example, the circuit in the left of Fig. 1 corresponds to a tensor $\frac{1}{\sqrt{2^4}} \sum_{x_5} (-1)^{f_C(x_1, x_2, \dots, x_7)}$ where

$$f_C(x_1, x_2, \dots, x_7) = x_1x_4 + x_2x_5 + x_3x_5 \\ + x_3x_4x_5 + x_4 + x_5x_6 + x_3x_7 + x_4x_6x_7.$$

We call this summation the *sum-of-powers* form for the circuit. In this example, x_5 is the only variable summed over in the expression.

Generally, for a circuit using gates from set \mathcal{Z} , the sum-of-powers form is $\frac{1}{\sqrt{2^h}} \sum_y (-1)^{f_C(x, y)}$, where h is the number of H gates and y stands for the internal variables. We define -1 as the *base* of the sum-of-powers forms above and *modulus* as the smallest positive integer exponent that brings the base to identity. The function f_C is a multilinear polynomial of degree at most three. For each H gate, the product of the input and output variables gives the term. While for Z, CZ, or CCZ gates, the product of the input variables gives the term.

3.2 Complex Gates

Not all elementary gates have the power form, but fortunately, there are different ways to work with them in the sum-of-powers framework. Consider the CNOT gate as an example, where $\text{CNOT} : |x_1, x_2\rangle \mapsto |x_1, x_1 \oplus x_2\rangle$. By definition, CNOT is a tensor that evaluates to 1 if the input variables x_1, x_2 and output variables y_1, y_2 satisfy $y_1 = x_1$ and $y_2 = x_1 \oplus x_2$ and to 0 otherwise. So one way to work with the CNOT gate is to label the wires with not just variables, but linear functions of variables. This approach was taken in [18], one of the early papers that used the wire labeling variables to analyze quantum circuits.

We take a different approach and use the fact that gates in \mathcal{Z} are universal so one can decompose CNOT as $(\text{I} \otimes \text{H}) \text{CZ} (\text{I} \otimes \text{H})$. See the right part of Fig. 1 for an illustration. A sum-of-powers form for CNOT is, therefore, $\frac{1}{2} \sum_y (-1)^{x_1y + x_2y + x_3y}$. It is easy to verify directly that if $x_3 = x_1 \oplus x_2$, the summation evaluates to 1 and otherwise evaluates to 0, which is consistent with the definition of CNOT. So the CNOT gate in the sum-of-powers form is represented by input variables x_1 and x_2 , output variables x_1 and x_3 , internal variable y and normalization factor 2. In this approach, gates obtained by such decompositions as the CNOT gate are called complex gates, whereas gates of the power form are called simple gates. The complex gates can be treated easily as the “syntactic sugar” of a sequence of simple gates in implementation.

We prefer this method because it is flexible and is much easier to implement. For example, it works with Toffoli gates as well where the Toffoli gate has input variables x_1, x_2, x_3 , output variables x_1, x_2, x_4 , and one internal variable y . The sum-of-powers form for Toffoli is $\frac{1}{2} \sum_y (-1)^{x_1x_2y + x_3y + x_4y}$. If we choose the first method using functions of variables as wire labels, multiple Toffoli gates will

induce high-degree polynomials in the general case, which may be even more difficult to implement.

3.3 Gate Set \mathcal{T}

All the sum-of-powers forms we have considered so far have modulus 2 and the functions f_C are effectively modulo 2. We emphasize that the modulus pertains to a sum-of-powers form of a gate, not the gate itself, as a single gate may admit multiple sum-of-powers representations with varying moduli.

We now expand our scope to the gate set $\mathcal{T} = \{\text{CNOT}, \text{H}, \text{T}\}$ and introduce sum-of-powers forms of base other than -1 . Let ω_8 be the 8-th root of unity $\omega_8 = e^{i\pi/4}$. The T gate is a diagonal matrix $\begin{pmatrix} 1 & 0 \\ 0 & \omega_8 \end{pmatrix}$. So in the sum-of-powers form, the input and output wire will have the same variable x and the T gate is represented as the power ω_8^x . The H gate has input and output variables x and y , respectively, as before, and has a power form $\omega_8^{4xy}/\sqrt{2}$. The CNOT gate has input x_1, x_2 and output variables x_1, x_3 as before and take the form $\frac{1}{2} \sum_y \omega_8^{4(x_1+x_2+x_3)y}$. In sum-of-powers representations, we work with the same base for all gates in the gate set. This is always possible to achieve by choosing the least common multiple of all the moduli of the gates as the common modulus, as we have done for the gate set \mathcal{T} .

3.4 Gate Set \mathcal{G}

In addition to the gate sets \mathcal{Z} and \mathcal{T} , the sum-of-powers framework is flexible enough to natively represent the gate set used in the Google supremacy experiment as well [8]. There, the gate set employed is \mathcal{G} which includes the single-qubit gates $\sqrt{X} = \frac{1}{\sqrt{2}} \begin{pmatrix} 1 & -i \\ -i & 1 \end{pmatrix}$, $\sqrt{Y} = \frac{1}{\sqrt{2}} \begin{pmatrix} 1 & -1 \\ 1 & 1 \end{pmatrix}$, $\sqrt{W} = \frac{1}{\sqrt{2}} \begin{pmatrix} 1 & -\sqrt{i} \\ \sqrt{-i} & 1 \end{pmatrix}$, and two-qubit gates

$$\text{fSim}(\pi/2, \pi/6) = \begin{pmatrix} 1 & & & \\ & 0 & -i & \\ & -i & 0 & \\ & & & e^{-i\pi/6} \end{pmatrix}, \quad \text{iSWAP} = \begin{pmatrix} 1 & & & \\ & 0 & -i & \\ & -i & 0 & \\ & & & 1 \end{pmatrix}.$$

The iSWAP is a simplified version of $\text{fSim}(\pi/2, \pi/6)$ often used in benchmarking BDD simulation methods. All these gates have the power form shown in Table 1, and the common modulus is 24.

We have introduced three distinct gate sets— \mathcal{Z} , \mathcal{T} , and \mathcal{G} —each characterized by its native gates. We summarize the discussion in the following theorem.

Theorem 1. *For any quantum circuit C of n qubits and m gates in universal gate sets \mathcal{Z} , \mathcal{T} , or \mathcal{G} , one can efficiently derive an SOP form $\frac{1}{\sqrt{R}} \sum_y \omega^{f(x,y)}$, representing the tensor of the circuit. In the representation, $f(x,y)$ is a multilinear polynomial of $\mathcal{O}(m)$ terms and degree at most three, and x corresponds to external variables assigned to the input and output wires of C .*

Table 1. Sum-of-powers representation for the Google supremacy gate set.

Gate	Input	Output	Representation	Factor
\sqrt{X}	x_0	x_1	$\omega_{24}^{18x_0+18x_1+12x_0x_1}$	$1/\sqrt{2}$
\sqrt{Y}	x_0	x_1	$\omega_{24}^{12x_0+12x_0x_1}$	$1/\sqrt{2}$
\sqrt{W}	x_0	x_1	$\omega_{24}^{15x_0+21x_1+12x_0x_1}$	$1/\sqrt{2}$
fSim($\pi/2, \pi/6$)	x_0, x_1	x_1, x_0	$\omega_{24}^{18x_0+18x_1+10x_0x_1}$	1
iSWAP	x_0, x_1	x_1, x_0	$\omega_{24}^{18x_0+18x_1+12x_0x_1}$	1

A key advantage of our method is its remarkable flexibility: the approach can be readily extended to new gate sets without requiring customized implementation, in contrast to previous methods like [50]. Supporting a new gate set becomes a simple matter of creating a configuration file that defines the coefficients, monomial terms, and other characteristics of the sum-of-powers representation for each gate in the set.

4 Tensor Contraction and Substitution on Sum-of-Powers

In the circuit simulation and equivalence checking problems discussed below, it is convenient to work with the sum-of-powers representations not only for circuits, but for other derived quantities such as $\langle a|U_C|0^n\rangle$ as well. These quantities are easy to formulate in the sum-of-powers framework given the following two operations of SOPs.

In tensor networks, the most important procedure for manipulating tensors is the tensor contraction operation, where two indices are identified and summed over [36]. For a sum-of-powers tensor $\sum_y \omega^{f(x,y)}$ and two external variables x_1 and x'_1 in x , it is natural to consider the *contraction* of variables x_1 and x'_1 . The resulting form is still a sum-of-powers tensor having the form $\sum_{x_1,y} \omega^{f[x_1/x'_1](x,y)}$, where $f[x_1/x'_1]$ is a function obtained by substituting all the variable x'_1 in f with x_1 . More generally, let x_1, x_2, \dots, x_k and x'_1, x'_2, \dots, x'_k be the different external variables that are contracted respectively, then the resulting sum-of-powers tensor is

$$\sum_{x_1, \dots, x_k, y} \omega^{f[x_1/x'_1, \dots, x_k/x'_k](x,y)},$$

where $f[x_1/x'_1, \dots, x_k/x'_k]$ is the function obtained by substituting x'_1, x'_2, \dots, x'_k with x_1, x_2, \dots, x_k respectively. Note that even though we write $f[x_1/x'_1, \dots, x_k/x'_k](x,y)$ but $f[x_1/x'_1, \dots, x_k/x'_k]$ is a function independent of x'_1, x'_2, \dots, x'_k .

Another procedure we need is variable *substitution*. Let $\sum_y \omega^{f(x,y)}$ be a sum-of-powers tensor, and let x_1, x_2, \dots, x_k be external variables in x . For any values $a_1, a_2, \dots, a_k \in \{0, 1\}$, the substitution of x_i with a_i for $i = 1, 2, \dots, k$ results in a sum-of-powers tensor $\sum_y \omega^{f[a_1/x_1, \dots, a_k/x_k](x,y)}$. This operation naturally arises when the wire corresponding to variable x_j is contracted with a basis state $|a_j\rangle$. The above discussions establish the following simple claim.

Theorem 2. *The contraction and substitution of an SOP result in another SOP.*

With the contraction and substitution operations established, we can now efficiently compute the sum-of-powers forms for the two quantities we require below. The first is the amplitude $\langle a|U_C|0^n \rangle$ where U_C is the unitary matrix for circuit C and $a \in \{0,1\}^n$ is a computation basis. Let $\frac{1}{R} \sum_y \omega^{f_C(x,y)}$ be the sum-of-powers tensor for circuit C . From Theorem 1, we know that f_C is a summation of $\mathcal{O}(m)$ monomial terms where m is the number of gates in the circuit.

Let $x^{\text{in}} = (x_1^{\text{in}}, x_2^{\text{in}}, \dots, x_n^{\text{in}})$ and $x^{\text{out}} = (x_1^{\text{out}}, x_2^{\text{out}}, \dots, x_n^{\text{out}})$ be the variables corresponding to the input and output qubits respectively. Each consists of n different variables, but they may share some common variables. This could happen, for example, when all gates acting on a qubit are diagonal, and the labeling strategy discussed in Section 3 will not introduce new variables for the qubit. Suppose there are $s \geq 0$ common variables in x^{in} and x^{out} and there are qubit indices j_1, \dots, j_s and k_1, \dots, k_s such that $x_{j_i}^{\text{in}} = x_{k_i}^{\text{out}}$ for all $i = 1, \dots, s$. Let k_{s+1}, \dots, k_n be the output qubit indices assigned non-common variables (that is, they are not in $\{k_1, \dots, k_s\}$). The sum-of-powers tensor for $\langle a|U_C|0^n \rangle$ is then 0 if there is an $i \in \{1, 2, \dots, s\}$ such that $a_{k_i} \neq 0$ (in other words, this constitutes a contradictory substitution, as a variable cannot simultaneously be substituted with both 0 and 1), or $\frac{1}{R} \sum_y \omega^{f'_C(y)}$ where

$$f'_C(y) = f_C[a_{k_{s+1}}/x_{k_{s+1}}^{\text{out}}, \dots, a_{k_n}/x_{k_n}^{\text{out}}, 0/x_1^{\text{in}}, \dots, 0/x_n^{\text{in}}](y).$$

This finishes the discussion on how to represent $\langle a|U_C|0^n \rangle$ as a sum-of-powers tensor network.

Next, we consider the representation for $\text{tr } U_C$. The basic idea is quite simple; we only need to perform a contraction of the input and output variables. Since an input variable may become an output variable on another qubit (e.g., the iSWAP gate in the gate set \mathcal{G}), we must ensure consistent substitution of each original variable during the contraction. Continuing with the above setup, consider the case that there are s common variables. Define a graph G of n vertices containing s edges (or self-loops) specified by $\{j_i, k_i\}$. Consider partitioning of the graph into t connected components G_1, G_2, \dots, G_t . Define a new variable z_j for each G_j where $j = 1, 2, \dots, t$. Suppose circuit C has the sum-of-powers form $\frac{1}{\sqrt{R}} \sum_y \omega^{f(x,y)}$. It is easy to convince oneself that the sum-of-powers form for $\text{tr } U_C$ is $\frac{1}{\sqrt{R}} \sum_{z,y} \omega^{f'_C(z,y)}$ where f' is the function obtained by substituting all external variables x in f_C using the following method. For each input variable x_i^{in} and output variable x_i^{out} , let G_{j_i} be the connected component to which vertex i belongs, and we substitute x_i^{in} and x_i^{out} with z_{j_i} .

5 FeynmanDD: Decision Diagram for Sum-of-Powers

In Sections 3 and 4, we presented methods for deriving sum-of-powers representations for circuit and quantities related to the circuit $\frac{1}{\sqrt{R}} \sum_y \omega^{f(x,y)}$, where R is a normalization factor, ω is the r -th root of unity, and $f : \{0,1\}^k \rightarrow \{0,1,\dots,r-1\}$

is a multilinear polynomial with values modulo r . The next step of the FeynmanDD method is to represent the function f using a variant of BDD called multi-terminal binary decision diagram (MTBDD).

As discussed in Section 1, FeynmanDD departs from most existing BDD-motivated approaches by utilizing classical decision diagrams as its underlying data structure. This strategy facilitates the immediate use of robust and efficient implementations developed over decades, including CUDD [49], BuDDy [34], Sylvan [20], and adiar [48]. Moreover, it seamlessly incorporates powerful variable ordering heuristics. CUDD and Sylvan offer multi-terminal support, rendering them suitable MTBDD engines for gate sets of any modulus. BuDDy and adiar currently support only standard BDDs and are consequently limited to gate sets with a modulus of 2. Our current implementation exclusively employs CUDD, leaving support for additional packages reserved for future development.

In many applications, it is possible to first represent the function f for the circuit C as an MTBDD and then try to compute the MTBDD for function f' for the derived quantities such as $\langle a|U_C|0^n \rangle$ or $\text{tr } U_C$. But the substitution and contraction usually help to simplify the multilinear polynomial significantly in the sum-of-powers and thereby also simplify its MTBDD representation. It is therefore preferred first to try to use methods in Theorem 2 to transform f at the polynomial representation level and delay the creation of the MTBDD as late as possible.

For instance, in the example circuit on the left part of Fig. 1, the function f_C has 7 variables and 8 terms. When representing it as a BDD, it has 28 nodes, including the constants 0 and 1. However, when enforcing the initial state condition, variables x_1, x_2, x_3 are set to 0, and the function reduces to one with 4 variables and 3 terms: $x_4 + x_5x_6 + x_4x_6x_7$. Its BDD is much smaller, containing only 10 nodes as shown in Fig. 2.

Given a function $f : \{0, 1\}^n \rightarrow [r]$ representing a multilinear polynomial of m terms

$$f(x) = \sum_{k=1}^m a_k x_1^{i_{k,1}} x_2^{i_{k,2}} \dots x_n^{i_{k,n}},$$

for $i_{k,j} \in \{0, 1\}$, we need to build the BDD representation of it from scratch. This represents the most computationally expensive step in our method. While the summation is commutative, the order of term addition can lead to dramatically different computational costs. To illustrate this phenomenon, consider a sequence of Hadamard gates. The polynomial f takes the form $\frac{r}{2} \sum_{j=0}^{k-1} x_j x_{j+1}$. When variables are ordered sequentially, the final BDD has a size of $\mathcal{O}(k)$. However, naive sequential term addition can result in a quadratic $\Omega(k^2)$ runtime, becoming inefficient for large k . The quadratic scaling emerges

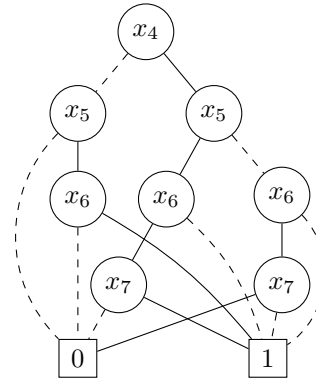


Fig. 2. BDD for the reduced function $x_4 + x_5x_6 + x_4x_6x_7$.

from the computational complexity of adding each term. Specifically, the time cost for combining the partial sum with the current term scales linearly with the MTBDD size of the partial sum. This linear scaling leads to a quadratic overall runtime through recursive addition. To address this efficiency challenge, we employ a *binary synthesis method*. This approach, utilizing the commutativity of addition modulo r , partitions terms into two groups of approximately equal size, first computes results within each group and then combines them. For the Hadamard sequence example, this reduces time complexity to $\mathcal{O}(k \log k)$. Numerical simulations suggest this binary synthesis method performs effectively across more generalized scenarios.

For the construction of a MTBDD, the second order that deserves careful consideration is the order of the variables in the decision diagram data structure as it may significantly impact the final size. Consider again the Hadamard sequence example: ordering the odd variables x_1, x_3, \dots first will cause the BDD size to grow exponentially. A well-know dynamic variable reordering heuristic is called sifting [45], which is supported by CUDD and is sometimes useful in the circuit classes used in Section 7. In our numerical experiments, we explore several other variable ordering heuristics to mitigate this challenge. For low-depth circuits, a pragmatic approach involves sequential qubit-based ordering. This method prioritizes variables by qubit, ordering all variables for the first qubit, then the second, and so on. We term this the *qubit order* strategy. For circuits with a small number of qubits, the *gate order* heuristics offer an effective variable ordering strategy. This approach ranks variables based on the first gate that employs them, providing a temporally informed sequence. An alternative method leverages standard tensor contraction optimization tools like *cotengra* to determine an optimal term order. Once this order is established, variables are arranged according to their appearance in the ordered terms. This approach, which we call the *tensor order* can sometimes be advantageous for random circuits. The concept of using tensor contraction complexity to bound BDD size has precedent in classical verification, where researchers previously explored the treewidth of CNF formulas [22]. Our approach diverges by focusing on the treewidth of XOR formulas. By employing these sophisticated ordering strategies, we can significantly optimize the efficiency of the MTBDD creation step.

The intuition behind the tensor contraction based heuristics is as follows. A fundamental fact about the size of a Boolean function f given variable order x_1, x_2, \dots, x_n is that the number of nodes with label x_i is the different number of functions $f[a_1/x_1, \dots, a_{i-1}/x_{i-1}]$ that essentially depends on x_i . This number is upper bounded by $O(2^{N_i})$ where N_i is the number of external wires in the process of contracting the sum-of-powers tensor network. While it is a useful ordering heuristics, its performance on linear-network circuits is poor, indicating that the tensor contraction complexity bound is an upper bound that may be very loose in certain cases.

Another useful technique for improving the efficiency of FeynmanDD is to use the counting identity $\sum_x (-1)^{xy+xz} = 2\delta_{y,z}$ to simplify the function f in the SOP. More specifically, when a variable x appears exactly twice in the terms

having form $\frac{r}{2}xx_0$ and $\frac{r}{2}xx_1$, we have

$$\frac{1}{\sqrt{R}} \sum_{x, x_0, x_1, y} \omega^{f(x, x_0, x_1, y)} = \frac{1}{\sqrt{R}} \sum_{x_0, x_1, y} \sum_x (-1)^{x(x_0 + x_1)} \omega^{f_{\text{rem}}(x_0, x_1, y)},$$

which simplifies to $\frac{2}{\sqrt{R}} \sum_{x_0, y} \omega^{f_{\text{rem}}[x_0/x_1](x_0, y)}$. This technique reduces the number of variables and therefore the size of the MTBDD and is most useful for simulating simple structured circuits.

On the technical level, CUDD does not support addition modulo r by default, and we implement a custom-made function for this and use CUDD's API `Cudd_addApply` to perform the operation on the data structure it maintains. Another technical issue worth mentioning is the requirement to handle high precision integers, as the counters involved for large circuits is huge. We implement a high precision counting algorithm for CUDD using the *GNU multiple precision arithmetic library*.

6 Quantum Circuit Analysis using FeynmanDD

6.1 Simulation of Quantum Circuits

In quantum circuit simulation, a fundamental problem is computing the amplitude $\langle a|C|0\rangle$ for a given $a \in \{0, 1\}^n$. This single amplitude simulation problem, which appears straightforward, is actually BQP-complete even for an approximation and $a = 0^n$. Considering a multilinear polynomial f representing the sum-of-powers representation of $\langle a|C|0\rangle$ with size $B(f)$, our simulation algorithm achieves runtime linear in $B(f)$. Consequently, when the multi-terminal binary decision diagram (MTBDD) representing f is small, we can effectively solve this problem.

The core algorithm reduces the evaluation of the sum-of-powers form to a finite number of counting problems on the MTBDD. By rewriting the amplitude SOP representation, we can express it as

$$\frac{1}{\sqrt{R}} \sum_y \omega^{f(y)} = \frac{1}{\sqrt{R}} \sum_{j=0}^{r-1} N_j \omega^j,$$

where $N_j = |\{y \mid f(y) \equiv j \pmod{r}\}|$ represents the number of inputs to f that evaluate to $j \in \{0, 1, \dots, r-1\}$. Given the MTBDD representing f , there are algorithms that can count the numbers N_j in time $\mathcal{O}(mB(f))$ where m is the bit length of the counting result [31, 58]. The number m is bounded by the number of gates, but usually much smaller and can often be considered constant in practice.

In quantum circuit simulation, another common task is computing the acceptance probability for a quantum circuit. Consider a circuit C acting on the initial state $|0^n\rangle$, with its sum-of-powers representation expressed as $\frac{1}{\sqrt{R}} \sum_y \omega^{f(x, y)}$, where x represents variables labeling the output qubits, the task is to estimate the probability of observing 1 when measuring the first qubit. We introduce a derived function $F(x, y, y') = f(x, y) - f(x, y')$ that operates on variables x, y, y' ,

with y' being a new set of variables matching y 's size. By defining x_1 as the variable of the qubit to be measured and $x_{>1}$ as the remaining variables, the acceptance probability can be formulated as:

$$\begin{aligned}\Pr(C \text{ accepts}) &= \langle 0^n | C^\dagger (|1\rangle\langle 1| \otimes I) C | 0^n \rangle \\ &= \frac{1}{R} \sum_{x_{>1}, y, y'} \omega^{f[1/x_1](x_{>1}, y) - f[1/x_1](x_{>1}, y')} \\ &= \frac{1}{R} \sum_{x_{>1}, y, y'} \omega^{F[1/x_1](x_{>1}, y, y')},\end{aligned}$$

where the contraction and substitution operations of SOPs are employed. Hence, the probability can be represented as $\frac{1}{R} \sum_z \omega^{F[1/x_1](z)}$ for $z = (x_{>1}, y, y')$. Notice that $B(F[1/x_1]) \leq B(F) \leq \mathcal{O}(B(f)^2)$, the algorithm has a quadratic complexity in terms of $B(f)$. In practice, we indeed observe that it is much less efficient compared with the linear complexity of the amplitude computation task. Yet, its performance is still comparably well for many circuit families.

Using a similar technique, we can estimate joint probabilities of measuring output qubits corresponding to variables x_1, \dots, x_j as

$$\Pr[x_1 = a_1, \dots, x_j = a_j] = \frac{1}{R} \sum_{x_{>j}, y, y'} \omega^{F[a_1/x_1, \dots, a_j/x_j](x_{>j}, y, y')},$$

where $x_{>j}$ are the remaining variables in x excluding x_1, \dots, x_j . This allows us to compute the conditional probabilities using the conditional probability formula

$$\Pr[x_j = a_j \mid x_1 = a_1, \dots, x_{j-1} = a_{j-1}] = \frac{\Pr[x_1 = a_1, \dots, x_j = a_j]}{\Pr[x_1 = a_1, \dots, x_{j-1} = a_{j-1}]}.$$

for all j and $a_1, a_2, \dots, a_j \in \{0, 1\}$. We can leverage this method to sample from the output distribution of $C|0^n\rangle$ using a simple sequential sampling algorithm. The process begins by computing the probability $p_1 = \Pr[x_1 = 0]$ and sampling the first bit with probabilities p_1 and $1 - p_1$. For subsequent bits, we compute $p_j = \Pr[x_j = 0 \mid x_1 = a_1, \dots, x_{j-1} = a_{j-1}]$ and sample accordingly. By repeating this process for $j = 2, 3, \dots, n$, we complete the sampling of all n output bits.

We remark that even though our simulation method requires a discrete universal gate set and cannot deal with arbitrary single-qubit rotations directly, it is possible to work with such circuits by expanding the rotations using Solovay-Kitaev theorem [17] or methods in [24, 44] to a sequence of, for example, H and T gates. As H will create a new variable and T gates will not, the gate sequence will introduce terms of the form $\frac{\tau}{2} \sum_{j=1} x_j x_{j+1} + \ell(x)$ where x_2, x_3, \dots are new variables introduced by the H gates and $\ell(x)$ is a linear function. By ordering x_2, x_3, \dots after x_1 , the resulting BDD will have a size not very sensitive to the length of the gate sequence.

6.2 Circuit Equivalence Checking

Circuit equivalence checking is another important task for quantum circuit analysis and optimization [27, 28, 43]. Usually, BDD-based methods are ideal for

such a task thanks to the uniqueness of BDD representations, and the circuit equivalence checking problem is reduced to check whether the BDDs for two circuits are identical. In our case, however, the BDD's for equivalent circuits may be dramatically different as it is based on the classical syntactical description of the circuit, not the semantic meaning (the unitary operator) of the circuit.

Fortunately, however, we are still able to use FeynmanDD to compute the trace of the unitary operator $\text{tr} U_C$ for circuit C . Given two circuits C_0, C_1 of n qubits, $\text{tr}(U_{C_0}^\dagger U_{C_1}) = 2^n \omega^j$ for some j , if and only if C_0 and C_1 are equivalent. This is a fact that was utilized in many previous works on circuit equivalence checking [28, 43]. Our method is then to first obtain the sum-of-powers form for $\frac{1}{2^n} \text{tr}(U_{C_0}^\dagger U_{C_1})$ and build the corresponding FeynmanDD for it as explained in Section 5. And the counting based method as in Section 6.1 is used for circuit simulation to evaluate the sum-of-powers form. We know that the two circuits are equivalent (up to a global phase) if the value has a unit norm. By using the multiple precision arithmetic library, the computation is performed exactly which is crucial for the equivalence checking application. Numerical experiments on using FeynmanDD for equivalence checking are discussed in Section 8.

7 Circuit Simulation Experiments and Comparisons

To evaluate the performance of FeynmanDD, we conducted a series of experiments comparing it with (a) three state-of-the-art quantum circuit simulators, DDSIM [62, 63], SliQSim [50], and WCFLOBDD [46, 47] and (b) MQT-QCEC (<https://github.com/cda-tum/qcec>) for the task of equivalence checking, a widely used tool that integrates multiple equivalence checking techniques. The experiments were performed on a server equipped with two Intel (R) Xeon (R) Platinum 8358P CPUs @ 2.60 GHz (64 cores, 128 threads in total) and 512 GB of memory. However, as CUDD does not support parallel computing, each simulation is performed using a single thread and our method barely uses more than 1 GB of memory.

Our numerical experiments cover three types of computational tasks: (1) the calculation of the amplitude $\langle 0|U|0\rangle$, (2) the simulation of sampling a full computational-basis measurement outcome, and (3) the equivalence checking of two given circuits. Furthermore, in the amplitude and sampling tasks, we measured the runtime and peak memory usage during the execution of these tasks by the program. Each simulation was limited to 3600 seconds (1 hour). For simplicity, we use qubit order to arrange the variables in all our experiments.

We tested four different families of circuits for quantum circuit simulation tasks: Google supremacy circuits, GHZ circuits, BV circuits, and a specially constructed family called linear-network circuits. The results are summarized in Tables 2 to 6. We present the comparison of circuit equivalence checking experiments in Section 8.

7.1 Google Supremacy Circuits

We used benchmarks from the GRCS repository⁴: `cz_v2` and `is_v1` circuits. The gate sets are $\{H, \sqrt{X}, \sqrt{Y}, T, CZ\}$ and $\{H, \sqrt{X}, \sqrt{Y}, T, iSWAP\}$ respectively. Since SliQSim does not natively support `iSWAP`, the corresponding results in Tables 2 and 3 were obtained via the decomposition

$$iSWAP = (S \otimes S)(H \otimes I)CNOT_{0,1}CNOT_{1,0}(I \otimes H).$$

For WCFLOBDD, since it does not natively support $Rx(\frac{\pi}{2})$ and $Ry(\frac{\pi}{2})$, we decomposed them as $Rx(\frac{\pi}{2}) = HSH$ and $Ry(\frac{\pi}{2}) = HZ$. Moreover, since WCFLOBDD provides only an interface for computing probabilities rather than amplitudes, and this interface did not function correctly in our tests, we conducted only the **Single Sample Output** test for WCFLOBDD. Each benchmark consists of ten circuits, and the table reports the average time and memory usage across these ten circuits.

FeynmanDD significantly outperformed DDSIM, SliQSim, and WCFLOBDD in runtime and memory usage. For `cz_v2` circuits, FeynmanDD was much faster and consumed less memory. Larger `cz/5x5_10` circuits timed out for DDSIM, SliQSim, and WCFLOBDD, while FeynmanDD completed within 0.05 seconds for amplitude estimation and 95 seconds for sampling. Due to excessive memory consumption, WCFLOBDD was severely limited in this test. Similar results were observed for `is_v1` circuits.

7.2 GHZ and BV Circuits

We tested two types of circuits in this part: GHZ circuits and BV circuits. GHZ circuits generate n -qubit GHZ states, while BV circuits implement the Bernstein-Vazirani algorithm with the all-ones secret string. These circuits were chosen as they generate simple yet highly entangled states.

As shown in Tables 4 and 5, FeynmanDD performed better than DDSIM and SliQSim in terms of both time and memory usage. The results confirm that FeynmanDD is capable of efficiently simulating these relatively simple circuits and can handle larger sizes of GHZ and BV circuits with little additional cost. In these tests, WCFLOBDD achieves the fastest runtime, while its memory usage is significantly higher than that of FeynmanDD.

7.3 Linear Network Circuits

These are IQP circuits based on degree-3 polynomials [39] $f : \{0, 1\}^n \rightarrow \{0, 1\}$ as follows:

$$f(x) = A(x) \sum_{i=1}^n x_i + \sum_{i=1}^{n-k+1} C_{i:i+k-1}, \quad (2)$$

⁴ <https://github.com/sboixo/GRCS>

Table 2. Quantum circuit simulation benchmarks on Google supremacy circuits for the task of zero to zero amplitude computation. In this and the following tables, n stands for the number of qubits, m is the number of gates, time is in seconds (s), memory is in MB, TO means timeout.

Circuit	n	m	Zero to Zero Amplitude					
			DDSIM		SliQSim		Ours	
			Time	Mem	Time	Mem	Time	Mem
cz/4x4_10	16	115	0.64	48.0	5.8	81.3	0.01	12.1
cz/4x5_10	20	145	67.6	362.3	666.9	255.5	0.03	12.2
cz/5x5_10	25	184	TO		TO		0.04	12.2
is/4x4_10	16	115	1.0	55.7	10.6	128.1	0.03	12.3
is/4x5_10	20	145	158.2	477.5	976.9	245.4	0.1	15.1
is/5x5_10	25	184	TO		TO		0.2	20.9

Table 3. Quantum circuit simulation benchmarks on Google supremacy circuits for the task of sampling. The (x) mark indicates that x tests timeout among the ten circuits tested in the group, and the shown value is derived from the average of the remaining $10 - x$ test results.

Circuit	n	m	Single Output Sample							
			DDSIM		SliQSim		WCFLOBDD		Ours	
			Time	Mem	Time	Mem	Time	Mem	Time	Mem
cz/4x4_10	16	115	0.53	48.00	6.10	153.53	184.32	18160.96	4.94	42.76
cz/4x5_10	20	145	71.65	362.31	785.91	355.38	TO		34.66	101.94
cz/5x5_10	25	184	TO		TO		TO		94.63	132.98
is/4x4_10	16	115	1.05	55.72	12.74	163.16	259.91	22349.67	7.62	76.02
is/4x5_10	20	145	178.52	477.57	1020.1	378.28	TO		25.36	116.72
is/5x5_10	25	184	TO		TO		TO		153.20(1)	156.15

Table 4. Quantum circuit simulation benchmarks on BV circuits. Time is measured in seconds (s), memory usage is measured in MB.

Qubits	Gates	Zero to Zero Amplitude						Single Output Sample							
		DDSIM		SliQSim		Ours		DDSIM		SliQSim		WCFLOBDD		Ours	
		Time	Mem	Time	Mem	Time	Mem	Time	Mem	Time	Mem	Time	Mem	Time	Mem
100	299	0.002	71.4	0.05	14.5	0.005	12.2	Error		0.05	14.62	0.04	480.02	0.007	14.54
500	1499	0.04	272.2	3.7	66.0	0.06	12.1			3.96	66.15	0.12	487.08	0.12	13.98
1000	2999	0.3	531.7	104.6	116.1	0.2	13.4			118.02	116.53	0.23	496.66	0.47	13.98
5000	14999	19.5	2540	506.0	234.1	5.8	65.9			520.05	234.93	1.21	592.82	10.27	17.39
10000	29999	138.7	5051	394.3	396.4	24.2	98.0			367.66	398.11	2.37	717.26	42.74	28.49

Table 5. Quantum circuit simulation benchmarks on GHZ circuits. Time is measured in seconds (s), memory usage is measured in MB.

Qubits	Gates	Zero to Zero Amplitude						Single Output Sample							
		DDSIM		SliQSim		Ours		DDSIM		SliQSim		WCFLOBDD		Ours	
		Time	Mem	Time	Mem	Time	Mem	Time	Mem	Time	Mem	Time	Mem	Time	Mem
100	100	0.0019	71.2	0.01	12.5	0.0023	12.2	0.002	71.29	0.009	14.19	0.03	478.84	0.005	13.98
500	500	0.04	271.8	0.07	23.9	0.01	12.3	0.04	271.72	0.06	24.36	0.04	479.87	0.05	13.98
1000	1000	0.3	530.3	0.9	48.2	0.04	12.8	0.26	530.34	0.91	48.93	0.06	481.52	0.18	13.98
5000	5000	19.9	2535	17.2	192.4	1.4	64.5	19.58	2535.00	18.73	193.14	0.22	495.71	4.14	13.98
10000	10000	142.1	5041	74.9	324.6	6.2	66.7	144.98	5041.17	78.12	326.00	0.43	512.53	16.68	18.71

where $A(x) := \sum_{i=1}^n \alpha_i x_i$, with α_i randomly selected from $\{0, 1\}$ and $k = \mathcal{O}(\log n)$. $C_{i:j}$ consists exclusively of degree-3 terms involving variables x_i, \dots, x_j . The design purposefully ensures that the second term $C_{i:i+k-1}$ involves k consecutive variables, guaranteeing that the number of forward signals for each module in Figure 23 of [31] remains bounded by $k + 1$. An important reason to include the $C_{i:i+k-1}$ terms in this construction is that they are implemented using CCZ gates, which are non-Clifford and prevent the use of the Gottesman-Knill algorithm [2, 25]. A more comprehensive analysis of this circuit family will be presented in subsequent work. For each (n, k) pair, ten circuits were generated. The values (including the number of gates) in Table 6 are the average values.

Table 6 demonstrates FeynmanDD’s strength in simulating linear-network circuits. For fixed n , increasing k moderately increased FeynmanDD’s runtime, but still much faster than DDSIM. For instance, when $n = 30$, $k = 7$ in amplitude task, FeynmanDD took 0.003s and 12MB, while DDSIM required approximately 1065s and 662MB on average. For the simulation task, FeynmanDD took 1s and 26MB while DDSIM used 1428s and 722MB on average. In contrast, WCFLOBDD was unable to complete the computation within one hour.

Table 6. Quantum circuit simulation benchmarks on linear-network circuits. In the table n is the number of qubits, k is a constant measuring gate locality. Time is measured in seconds (s), memory usage is measured in MB. SliQSim is not compared as it currently does not support CCZ gates.

n	k	Gates	Zero to Zero Amplitude				Single Output Sample					
			DDSIM		Ours		DDSIM		WCFLOBDD		Ours	
			Time	Mem	Time	Mem	Time	Mem	Time	Mem	Time	Mem
20	5	162.0	0.20	34.17	0.002	12.15	0.19	34.21	187.06	12466.84	0.14	13.79
20	7	163.0	0.30	38.20	0.003	12.13	0.29	38.23	464.12	21069.78	0.64	16.74
30	5	319.8	459.07 (1)	157.49	0.003	12.13	460.53 (1)	157.56	TO		0.34	13.92
30	7	321.1	1065.42 (4)	662.17	0.003	12.14	1428.32 (3)	721.57	TO		1.00	26.06
40	5	527.3	TO		0.004	12.17	TO		TO		0.75	26.63
40	7	531.7	TO		0.005	12.13	TO		TO		1.60	35.47

8 Circuit Equivalence Checking Experiments and Results

We evaluated the performance of FeynmanDD for the task of equivalence checking by comparing it with MQT-QCEC (<https://github.com/cda-tum/qcec>), a widely used tool that integrates multiple equivalence checking techniques. To conduct the tests, both input circuits needed to use discrete gate sets supported by FeynmanDD. Specifically, we selected (1) a subset of quantum circuits from RevLib [60] that FeynmanDD can process and (2) some quantum circuits used in Section 7. The experimental setup followed the same configuration as described in Section 7. The time limit for each check was set to 600 seconds (10 minutes).

Following convention in the literature, we considered three types of equivalence checking tasks:

Table 7. Quantum circuit equivalence check benchmarks. n stands for the number of qubits, m is the number of gates of original circuit, m' is the number of gates of transformed circuit, time is in seconds (s), TO means timeout.

Circuit	n	m	m'	Equivalent		Missing		Reverse	
				MQT-QCEC	Ours	MQT-QCEC	Ours	MQT-QCEC	Ours
0410184_169	14	46	46	1.73	0.08	1.51	0.32	1.25	0.43
4gt11-v1_85	5	8	8	0.45	0.02	0.32	0.02	0.45	0.02
alu-v0_27	5	11	11	0.49	0.02	0.48	0.01	0.46	0.01
alu-v1_29	5	12	12	0.54	0.02	0.44	0.02	0.37	0.003
alu-v2_33	5	12	12	0.08	0.002	0.06	0.002	0.06	0.002
alu-v3_35	5	12	12	0.08	0.002	0.07	0.002	0.07	0.002
alu-v4_37	5	12	12	0.18	0.002	0.16	0.003	0.12	0.003
apex2_289	498	1785	1779	38.13	TO	36.36	TO	137.44	TO
avg16_324	576	3996	3996	57.39	TO	TO	TO	TO	TO
avg8_325	320	2013	2013	27.39	TO	TO	TO	TO	TO
bw_291	87	312	312	0.90	2.33	0.96	3.39	TO	6.80
c2_181	35	116	116	2.87	TO	0.56	81.36	2.60	TO
cps_292	923	2787	2779	35.76	TO	27.50	TO	TO	TO
cycle10_293	39	90	88	3.13	0.03	3.21	0.02	5.04	0.06
e64-bdd_295	195	452	452	13.78	0.41	28.31	0.20	13.22	0.18
ham7_106	7	32	32	1.92	4.15	2.28	2.53	1.80	4.02
ham7_299	21	68	62	0.59	0.01	0.77	0.005	0.69	0.005
pdc_307	619	2096	2096	11.52	TO	11.60	TO	412.45	TO
spla_315	489	1725	1725	34.94	TO	21.39	TO	27.96	TO
sym6_316	14	35	35	1.08	0.02	0.98	0.03	0.98	0.03
sym9_317	27	71	71	3.05	0.12	1.87	0.27	3.17	0.38
GHZ_100	100	100	100	4.88	0.01	4.96	0.01	5.00	0.01
GHZ_500	500	500	500	13.22	0.35	13.47	0.32	13.29	0.47
GHZ_1000	1000	1000	1000	15.16	1.35	15.04	1.49	15.29	1.21
GHZ_5000	5000	5000	5000	311.40	26.10	354.13	26.36	320.29	25.71
GHZ_10000	10000	10000	10000	TO	91.53	TO	91.72	TO	89.18
BV100	100	299	299	4.03	0.04	4.22	0.08	4.58	0.04
BV500	500	1499	1499	13.27	0.79	13.57	0.88	13.88	0.78
linear_20_5_1_0	20	208	184	1.96	0.01	1.76	0.01	No CNOT	
linear_20_7_1_0	20	205	181	1.99	0.005	3.71	0.004		
linear_30_5_1_0	30	380	346	2.58	0.03	2.76	0.02		
linear_30_7_1_0	30	407	369	2.05	0.01	5.15	0.03		
linear_40_5_1_0	40	645	601	2.48	0.02	2.01	0.02		
linear_40_7_1_0	40	596	540	3.39	0.01	4.06	0.01		
cz_v2/4x4_10	16	115	181	1.24	0.29	1.34	0.42	No CNOT	
cz_v2/4x5_10	20	145	229	0.73	0.93	0.74	0.91		
cz_v2/5x5_10	25	184	289	0.78	1.01	0.46	1.34		
cz_v2/4x4_5	16	61	100	0.83	0.005	0.58	0.01		
cz_v2/4x5_5	20	79	132	0.92	0.01	1.03	0.01		
cz_v2/5x5_5	25	99	164	1.37	0.01	1.34	0.01		
cz_v2/5x6_5	30	120	199	1.42	0.04	1.45	0.06		
cz_v2/6x6_5	36	144	238	1.50	0.24	1.52	0.22		

1. *Equivalent*: Confirming equivalence between the original and transformed circuits. We used the `transpile` function in Qiskit with an optimization level of *O3* to generate transformed circuits. For Google supremacy circuits, the transformed basic gate set was specified as $\{H, Z, Rz, CZ\}$, which sometimes led to an increased gate count compared to the original.
2. *Missing*: Randomly removing one gate from the transformed circuit obtained in (1) and checking its difference with the original circuit.
3. *Reverse*: For transformed circuits containing CNOT gates after (1), we randomly selected one CNOT gate and swapped its control and target qubits, then checked for differences between the modified and original circuits. If no CNOT gates were present, this task was not performed.

The results are summarized in Table 7, which reports execution times for both programs. They demonstrate that FeynmanDD generally outperforms in equivalence checking tasks when applied to the quantum circuits from Section 7. For instance, in tests with GHZ circuits, FeynmanDD runs significantly faster than MQT-QCEC. When evaluating circuits from RevLib, FeynmanDD also shows superior performance in some cases. However, for certain RevLib circuits, particularly those with numerous gates, FeynmanDD’s performance is less satisfactory.

9 Summary

In summary, FeynmanDD represents a new method for quantum circuit analysis, building upon the Feynman path integral concept and decision diagram-based counting algorithms. The approach transforms circuits with a supported gate set into specialized tensor networks—proposed as sum-of-powers forms—effectively reducing many quantum circuit simulation tasks to counting problems. The method converts quantum circuits to multi-terminal BDDs and computes quantities of interest by counting function values modulo a constant. Experimental results demonstrate superior performance in single amplitude computation compared to existing decision diagram methods. FeynmanDD also delivers competitive performance in multi-qubit measurement string sampling and equivalence checking, successfully completing certain computations that remain intractable for other approaches.

This research reveals several promising future directions. First, it would be interesting to explore approximation techniques to complement the current exact computation approach, potentially enabling scaling to larger systems. Second, alternative methods for handling complex gates like CNOT could be investigated, such as using linear function labels for variables instead of introducing additional variables. Third, further improvements might be achieved through more comprehensive circuit simplification techniques, which were minimally utilized in our implementation. Fourth, the implementation could expand beyond CUDD, potentially adopting Sylvan as an alternative support package to leverage parallel computing capabilities. Given that memory usage is not currently the bottleneck, such a transition may yield significant performance improvements for large circuits. Finally, this technique shows promise for broader quantum computing applications, including quantum device validation, performance benchmarking, quantum circuit simplification, and verifiable quantum advantage.

Acknowledgments

The work is supported by National Key Research and Development Program of China (Grant No. 2023YFA1009403), National Natural Science Foundation of China (Grant No. 12347104), Beijing Natural Science Foundation (Grant No. Z220002), Zhongguancun Laboratory, and Tsinghua University. BC acknowledges the support by the National Research Foundation, Singapore, and A*STAR under

its CQT Bridging Grant and its Quantum Engineering Programme under grant NRF2021-QEP2-02-P05.

References

1. Aaronson, S., Arkhipov, A.: The Computational Complexity of Linear Optics. *Theory of Computing* **9**(1), 143–252 (2013). <https://doi.org/10.4086/toc.2013.v009a004>
2. Aaronson, S., Gottesman, D.: Improved Simulation of Stabilizer Circuits. *Physical Review A* **70**(5), 052328 (2004). <https://doi.org/10.1103/PhysRevA.70.052328>
3. Abdollahi, A., Pedram, M.: Analysis and Synthesis of Quantum Circuits by Using Quantum Decision Diagrams. In: *Proceedings of the Design Automation & Test in Europe Conference*. pp. 1–6. IEEE, Munich, Germany (2006). <https://doi.org/10.1109/date.2006.244176>
4. Abdulla, P.A., Chen, Y.G., Chen, Y.F., Holík, L., Lengál, O., Lin, J.A., Lo, F.Y., Tsai, W.L.: Verifying Quantum Circuits with Level-Synchronized Tree Automata. *Verifying Quantum Circuits with Level-Synchronized Tree Automata* **9**(POPL), 32:923–32:953 (2025). <https://doi.org/10.1145/3704868>
5. Amy, M.: *Formal Methods in Quantum Circuit Design*. Ph.D. thesis, University of Waterloo (2019)
6. Amy, M.: Towards Large-scale Functional Verification of Universal Quantum Circuits. *Electronic Proceedings in Theoretical Computer Science* **287**, 1–21 (2019). <https://doi.org/10.4204/EPTCS.287.1>
7. Amy, M.: Complete equational theories for the sum-over-paths with unbalanced amplitudes. *Electronic Proceedings in Theoretical Computer Science* **384**, 127–141 (2023). <https://doi.org/10.4204/eptcs.384.8>
8. Arute, F., Arya, K., Babbush, R., Bacon, D., Bardin, J.C., Barends, R., Biswas, R., Boixo, S., Brandao, F.G.S.L., Buell, D.A., Burkett, B., Chen, Y., Chen, Z., Chiaro, B., Collins, R., Courtney, W., Dunsworth, A., Farhi, E., Foxen, B., Fowler, A., Gidney, C., Giustina, M., Graff, R., Guerin, K., Habegger, S., Harrigan, M.P., Hartmann, M.J., Ho, A., Hoffmann, M., Huang, T., Humble, T.S., Isakov, S.V., Jeffrey, E., Jiang, Z., Kafri, D., Kechedzhi, K., Kelly, J., Klimov, P.V., Knysh, S., Korotkov, A., Kostritsa, F., Landhuis, D., Lindmark, M., Lucero, E., Lyakh, D., Mandrà, S., McClean, J.R., McEwen, M., Megrant, A., Mi, X., Michielsen, K., Mohseni, M., Mutus, J., Naaman, O., Neeley, M., Neill, C., Niu, M.Y., Ostby, E., Petukhov, A., Platt, J.C., Quintana, C., Rieffel, E.G., Roushan, P., Rubin, N.C., Sank, D., Satzinger, K.J., Smelyanskiy, V., Sung, K.J., Trevithick, M.D., Vainsencher, A., Villalonga, B., White, T., Yao, Z.J., Yeh, P., Zalcman, A., Neven, H., Martinis, J.M.: Quantum supremacy using a programmable superconducting processor. *Nature* **574**(7779), 505–510 (2019). <https://doi.org/10.1038/s41586-019-1666-5>
9. Bahar, R., Frohm, E., Gaona, C., Hachtel, G., Macii, E., Pardo, A., Somenzi, F.: Algebraic decision diagrams and their applications. In: *Proceedings of 1993 International Conference on Computer Aided Design (ICCAD)*. pp. 188–191. IEEE Comput. Soc. Press, Santa Clara, CA, USA (1993). <https://doi.org/10.1109/iccad.1993.580054>
10. Bryant, R.E.: Graph-Based Algorithms for Boolean Function Manipulation. *IEEE Transactions on Computers* **C-35**(8), 677–691 (1986). <https://doi.org/10.1109/tc.1986.1676819>
11. Bryant, R.: Binary decision diagrams and beyond: enabling technologies for formal verification. In: *Proceedings of IEEE International Conference on Computer Aided Design (ICCAD)*. pp. 236–243. IEEE Comput. Soc. Press, San Jose, CA, USA (1995). <https://doi.org/10.1109/iccad.1995.480018>
12. Burgholzer, L., Bauer, H., Wille, R.: Hybrid Schrödinger-Feynman Simulation of Quantum Circuits With Decision Diagrams. In: *2021 IEEE International Conference*

- on Quantum Computing and Engineering (QCE). pp. 199–206. IEEE, Broomfield, CO, USA (2021). <https://doi.org/10.1109/QCE52317.2021.00037>
13. Chareton, C., Bardin, S., Bobot, F., Perrelle, V., Valiron, B.: An automated deductive verification framework for circuit-building quantum programs. In: Programming Languages and Systems: 30th European Symposium on Programming, ESOP 2021, Held as Part of the European Joint Conferences on Theory and Practice of Software, ETAPS 2021, Luxembourg City, Luxembourg, March 27 – April 1, 2021, Proceedings. pp. 148–177. Springer-Verlag, Berlin, Heidelberg (2021). https://doi.org/10.1007/978-3-030-72019-3_6
 14. Chen, Y.F., Chung, K.M., Lengál, O., Lin, J.A., Tsai, W.L.: AutoQ: An Automata-Based Quantum Circuit Verifier. In: Enea, C., Lal, A. (eds.) Computer Aided Verification. pp. 139–153. Springer Nature Switzerland, Cham (2023). https://doi.org/10.1007/978-3-031-37709-9_7
 15. Coecke, B., Duncan, R.: Interacting Quantum Observables. In: Aceto, L., Damgård, I., Goldberg, L.A., Halldórsson, M.M., Ingólfssdóttir, A., Walukiewicz, I. (eds.) Automata, Languages and Programming. pp. 298–310. Springer, Berlin, Heidelberg (2008). https://doi.org/10.1007/978-3-540-70583-3_25
 16. Coecke, B., Horsman, D., Kissinger, A., Wang, Q.: Kindergarden quantum mechanics graduates ...or how I learned to stop gluing LEGO together and love the ZX-calculus. Theoretical Computer Science **897**, 1–22 (2022). <https://doi.org/10.1016/j.tcs.2021.07.024>
 17. Dawson, C.: Solovay Kitaev algorithm (2019)
 18. Dawson, C.M., Hines, A.P., Mortimer, D., Haselgrove, H.L., Nielsen, M.A., Osborne, T.J.: Quantum computing and polynomial equations over the finite field \mathbb{Z}_2 . Quantum Info. Comput. **5**(2), 102–112 (2005)
 19. Deng, H., Tao, R., Peng, Y., Wu, X.: A case for synthesis of recursive quantum unitary programs. Proc. ACM Program. Lang. **8**(POPL) (2024). <https://doi.org/10.1145/3632901>
 20. van Dijk, T.: Sylvan: multi-core decision diagrams. PhD, University of Twente, Enschede, The Netherlands (2016). <https://doi.org/10.3990/1.9789036541602>
 21. Fenner, S., Green, F., Homer, S., Pruim, R.: Determining acceptance possibility for a quantum computation is hard for the polynomial hierarchy. Proceedings of the Royal Society of London. Series A: Mathematical, Physical and Engineering Sciences **455**(1991), 3953–3966 (1999). <https://doi.org/10.1098/rspa.1999.0485>
 22. Ferrara, A., Pan, G., Vardi, M.Y.: Treewidth in Verification: Local vs. Global. In: Sutcliffe, G., Voronkov, A. (eds.) Logic for Programming, Artificial Intelligence, and Reasoning. pp. 489–503. Lecture Notes in Computer Science, Springer, Berlin, Heidelberg (2005). https://doi.org/10.1007/11591191_34
 23. Feynman, R., Hibbs, A.: Quantum Mechanics and Path Integrals. International series in pure and applied physic, McGraw-Hill (1965)
 24. Giles, B., Selinger, P.: Exact synthesis of multiqubit Clifford+ T circuits. Physical Review A **87**(3), 032332 (2013). <https://doi.org/10.1103/physreva.87.032332>
 25. Gottesman, D.: The Heisenberg Representation of Quantum Computers. arXiv:quant-ph/9807006 (1998)
 26. Hillmich, S., Zulehner, A., Kueng, R., Markov, I.L., Wille, R.: Approximating Decision Diagrams for Quantum Circuit Simulation. ACM Transactions on Quantum Computing **3**(4), 22:1–22:21 (2022). <https://doi.org/10.1145/3530776>
 27. Hong, X., Feng, Y., Li, S., Ying, M.: Equivalence Checking of Dynamic Quantum Circuits. In: 2022 IEEE/ACM International Conference On Computer Aided Design (ICCAD). pp. 1–8 (2022)

28. Hong, X., Ying, M., Feng, Y., Zhou, X., Li, S.: Approximate Equivalence Checking of Noisy Quantum Circuits. In: 2021 58th ACM/IEEE Design Automation Conference (DAC). pp. 637–642 (2021). <https://doi.org/10.1109/DAC18074.2021.9586214>
29. Hong, X., Zhou, X., Li, S., Feng, Y., Ying, M.: A Tensor Network based Decision Diagram for Representation of Quantum Circuits. *ACM Trans. Des. Autom. Electron. Syst.* **27**(6), 60:1–60:30 (2022). <https://doi.org/10.1145/3514355>
30. Jiang, S., Fu, R., Burgholzer, L., Wille, R., Ho, T.Y., Huang, T.W.: FlatDD: A High-Performance Quantum Circuit Simulator using Decision Diagram and Flat Array. In: Proceedings of the 53rd International Conference on Parallel Processing. pp. 388–399. ICPP '24, Association for Computing Machinery, New York, NY, USA (2024). <https://doi.org/10.1145/3673038.3673073>
31. Knuth, D.E.: The Art of Computer Programming, Volume 4, Fascicle 1 (Bitwise Tricks & Techniques; Binary Decision Diagrams). AddisonWesley Professional, Upper Saddle River, NJ, 1 edition edn. (2009)
32. Larsen, C.B., Olsen, S.B., Larsen, K.G., Schilling, C.: Contraction Heuristics for Tensor Decision Diagrams. *Entropy* **26**(12), 1058 (2024). <https://doi.org/10.3390/e26121058>
33. Li, R., Wu, B., Ying, M., Sun, X., Yang, G.: Quantum supremacy circuit simulation on sunway taihulight. *IEEE Transactions on Parallel and Distributed Systems* **31**(4), 805–816 (2020). <https://doi.org/10.1109/TPDS.2019.2947511>
34. Lind-Nielsen, J.: Buddy : A binary decision diagram package. (1999)
35. Lu, C.Y., Wang, S.A., Kuo, S.Y.: An Extended XQDD Representation for Multiple-Valued Quantum Logic. *IEEE Transactions on Computers* **60**(10), 1377–1389 (2011). <https://doi.org/10.1109/TC.2011.114>
36. Markov, I.L., Shi, Y.: Simulating Quantum Computation by Contracting Tensor Networks. *SIAM Journal on Computing* **38**(3), 963–981 (2008). <https://doi.org/10.1137/050644756>
37. Mei, J., Bonsangue, M., Laarman, A.: Simulating Quantum Circuits by Model Counting (2024). <https://doi.org/10.48550/arXiv.2403.07197>
38. Molitor, P., Mohnke, J., Becker, B., Scholl, C.: Equivalence Checking of Digital Circuits: Fundamentals, Principles, Methods. Springer New York, NY (2004)
39. Montanaro, A.: Quantum circuits and low-degree polynomials over F_2 . *Journal of Physics A: Mathematical and Theoretical* **50**(8), 084002 (2017). <https://doi.org/10.1088/1751-8121/aa565f>
40. Nam, Y., Ross, N.J., Su, Y., Childs, A.M., Maslov, D.: Automated optimization of large quantum circuits with continuous parameters. *npj Quantum Information* **4**(1), 1–12 (2018). <https://doi.org/10.1038/s41534-018-0072-4>
41. Niemann, P., Wille, R., Miller, D.M., Thornton, M.A., Drechsler, R.: QMDDs: Efficient Quantum Function Representation and Manipulation. *IEEE Transactions on Computer-Aided Design of Integrated Circuits and Systems* **35**(1), 86–99 (2016). <https://doi.org/10.1109/tcad.2015.2459034>
42. Pan, F., Zhang, P.: Simulation of Quantum Circuits Using the Big-Batch Tensor Network Method. *Physical Review Letters* **128**(3), 030501 (2022). <https://doi.org/10.1103/PhysRevLett.128.030501>
43. Peham, T., Burgholzer, L., Wille, R.: Equivalence Checking of Quantum Circuits With the ZX-Calculus. *IEEE Journal on Emerging and Selected Topics in Circuits and Systems* **12**(3), 662–675 (2022). <https://doi.org/10.1109/JETCAS.2022.3202204>
44. Ross, N.J., Selinger, P.: Optimal ancilla-free Clifford+T approximation of z-rotations. *arXiv:1403.2975 [quant-ph]* (2016)

45. Rudell, R.: Dynamic variable ordering for ordered binary decision diagrams. In: Proceedings of 1993 International Conference on Computer Aided Design (ICCAD). pp. 42–47 (1993). <https://doi.org/10.1109/ICCAD.1993.580029>
46. Sistla, M., Chaudhuri, S., Reps, T.: Symbolic quantum simulation with quasimodo. In: Computer Aided Verification: 35th International Conference, CAV 2023, Paris, France, July 17–22, 2023, Proceedings, Part III. pp. 213–225. Springer-Verlag, Berlin, Heidelberg (2023). https://doi.org/10.1007/978-3-031-37709-9_11
47. Sistla, M., Chaudhuri, S., Reps, T.: Weighted Context-Free-Language Ordered Binary Decision Diagrams. Weighted CFLOBDDs **8**(OOPSLA2), 320:1390–320:1419 (2024). <https://doi.org/10.1145/3689760>
48. Sølvsten, S.C., van de Pol, J., Jakobsen, A.B., Thomasen, M.W.B.: Efficient Binary Decision Diagram Manipulation in External Memory. arXiv:2104.12101 [cs] (2021)
49. Somenzi, F.: CUDD: CU decision diagram package (release 3.0.0). University of Colorado at Boulder (2005)
50. Tsai, Y.H., Jiang, J.H.R., Jhang, C.S.: Bit-Slicing the Hilbert Space: Scaling Up Accurate Quantum Circuit Simulation. In: 2021 58th ACM/IEEE Design Automation Conference (DAC). pp. 439–444 (2021). <https://doi.org/10.1109/DAC18074.2021.9586191>
51. Viamontes, G.F., Markov, I.L., Hayes, J.P.: Improving Gate-Level Simulation of Quantum Circuits. Quantum Information Processing **2**(5), 347–380 (2003). <https://doi.org/10.1023/b:qinp.0000022725.70000.4a>
52. Viamontes, G.F., Markov, I.L., Hayes, J.P.: Checking equivalence of quantum circuits and states. In: 2007 IEEE/ACM International Conference on Computer-Aided Design. pp. 69–74. IEEE, San Jose, CA, USA (2007). <https://doi.org/10.1109/iccad.2007.4397246>
53. Vilmart, R.: The structure of sum-over-paths, its consequences, and completeness for clifford (2020)
54. Vilmart, R.: Completeness of sum-over-paths for toffoli-hadamard and the dyadic fragments of quantum computation (2022)
55. Vilmart, R.: Rewriting and completeness of sum-over-paths in dyadic fragments of quantum computing. Logical Methods in Computer Science **Volume 20, Issue 1** (2024). [https://doi.org/10.46298/lmcs-20\(1:20\)2024](https://doi.org/10.46298/lmcs-20(1:20)2024)
56. Vinkhuijzen, L., Grurl, T., Hillmich, S., Brand, S., Wille, R., Laarman, A.: Efficient Implementation of LIMDDs for Quantum Circuit Simulation. In: Caltais, G., Schilling, C. (eds.) Model Checking Software. pp. 3–21. Springer Nature Switzerland, Cham (2023). https://doi.org/10.1007/978-3-031-32157-3_1
57. Watrous, J.: Quantum Computational Complexity. In: Meyers, R.A. (ed.) Encyclopedia of Complexity and Systems Science, pp. 7174–7201. Springer, New York, NY (2009). https://doi.org/10.1007/978-0-387-30440-3_428
58. Wegener, I.: Branching programs and binary decision diagrams: theory and applications. SIAM monographs on discrete mathematics and applications, Society for Industrial and Applied Mathematics, Philadelphia (2000)
59. van de Wetering, J.: ZX-calculus for the working quantum computer scientist. arXiv:2012.13966 [quant-ph] (2020)
60. Wille, R., Große, D., Teuber, L., Dueck, G.W., Drechsler, R.: RevLib: An online resource for reversible functions and reversible circuits. In: Int’l Symp. on Multi-Valued Logic. pp. 220–225 (2008)
61. Wille, R., Hillmich, S., Burgholzer, L.: Tools for Quantum Computing Based on Decision Diagrams. ACM Transactions on Quantum Computing **3**(3), 13:1–13:17 (2022). <https://doi.org/10.1145/3491246>

62. Zulehner, A., Hillmich, S., Wille, R.: How to Efficiently Handle Complex Values? Implementing Decision Diagrams for Quantum Computing. arXiv:1911.12691 [quant-ph] (2019)
63. Zulehner, A., Wille, R.: Advanced Simulation of Quantum Computations. IEEE Transactions on Computer-Aided Design of Integrated Circuits and Systems **38**(5), 848–859 (2019). <https://doi.org/10.1109/tcad.2018.2834427>